Chapter 4

Robust Control of Atomic Force Microscopy

The atomic force microscope (AFM) is an instrument used for acquiring images at nanometer scale. Obtaining better image quality at higher scan speed is a research area of great interest in the control of an AFM. Improving the dynamic response of the scanning probe in the vertical direction and the dynamic response of the scanning motion in the lateral plane are the two major areas of application of advanced control methods to an AFM. The uncertainties inherent in the models of AFM vertical and lateral direction motion stages dictates the application of robust control methods. In this chapter, robust control methods are applied to AFM, treating first the vertical direction and then the lateral plane.

4.1. Introduction

Improvement in the AFM stage dynamics is achieved either by designing stages with higher bandwidth or by designing more sophisticated controllers rather than in the PI, PID, or PIID types of controllers that are most commonly used in practice. A robust repetitive controller is used for the vertical direction as it can reject higher frequency disturbances due to the periodic part of the surface topography in AFM much better than a conventional controller. Besides increasing the scan speed, it is also important that the phase lag can be compensated using repetitive control, with the knowledge of the surface topography from the previous period by introducing appropriate phase advance into the controller. Next, a multi-input–multi-output (MIMO) extension of the disturbance observer control method is applied to the

---

Chapter written by Bilin AKSUN GÜVENÇ, Serkan NECİPOĞLU, Burak DEMİREL and Levent GÜVENÇ.

Mechatronics Edited by J. Paulo Davim

lateral plane of scanning motion in a piezoelectric tube-based atomic force microscope (AFM). Calibration free and decoupled operation of the AFM is achieved with this technique. The technique is also robust to creep and hysteresis effects that are common in piezoelectric actuators. Both the repetitive and the MIMO disturbance observer controllers are designed using the control of mechatronic systems toolbox (COMES).

4.2. Repetitive control of the vertical direction motion

The AFM invented by Binnig *et al.* [BIN 86] is used for acquiring surface topography at the precision of nanometers. The selective features of AFM such as the ability of fast and easy sample preparation, air, liquid, and vacuum environments of operation, relatively lower costs, and so on make it an imaging technique of strong preference. Hence, improving the performance of AFM scanning has been an active area of research. The performance of an AFM can be described in terms of its scanning speed and image quality, which are inversely proportional to each other. The two major limitations imposed on scanning speed without violating the image quality and stability are the transient response of the cantilever probe and the mechanical bandwidth of the mechanisms used on the vertical axis "*z*", which are mostly made of piezoelectric actuators. These are followed by the general limitations of the feedback loop such as time delays, sampling rate in the case of digital control, sensor noise, RMS conversion rate, and so on. More information on AFM dynamics and control is given in [GAR 02] and [ABR 07]. Figure 4.1 shows a basic presentation of an AFM setup.

The transient response of the probe is quantified by the quality factor (Q) of the cantilever beam [SUL 02]. High Q values cause slow response of the probe to surface topographic changes and even instability in dynamic, amplitude modulated (AM) AFM, e.g. tapping mode. An active Q control to improve the response time is also proposed in [SUL 02]. An adaptive Q control (AQC) depending on the surface properties is proposed in [GUN 07], whereas a full state feedback control method affecting both Q and the resonant frequency of the vibrating probe is presented in [ORU 09].

It is very common among physicists to use a PI, PID, PII, or a PIID controller for the vertical motion of the scanner on *z*-direction [ABR 07]. Obviously, a simple PI controller cannot improve the bandwidth to perform good surface tracking at high frequencies. Adding a derivative term seems to be a good idea at first, but this is avoided because the measurement of the probe's deflection is noisy. However, the bandwidth of the scanner's vertical motion in the *z*-direction can be improved by using a more sophisticated mechanical design [SCH 07] or by implementing more advanced control techniques. Such an advanced controller is implemented in

[SCH 01] utilizing H_∞ control theory. Advanced robust controllers can handle the inevitable nonlinearities and system uncertainties as well.

When the continuity of the scanned surface is considered, it is reasonable to assume that the successive lines of the scan are similar. This motivates researchers to make use of past scanning information for improving the performance of the scan on following scan lines. The combination of feedforward and H_∞ controller is used in [SCH 04] for this purpose. Other feedforward, learning- and observer-based controllers are proposed in [SCH 04], [LI 08], [FUJ 08], and [SAL 05] for the periodic motions of the scanner. A brief discussion about the combination of feedback and feedforward controllers is presented in [PAO 07].

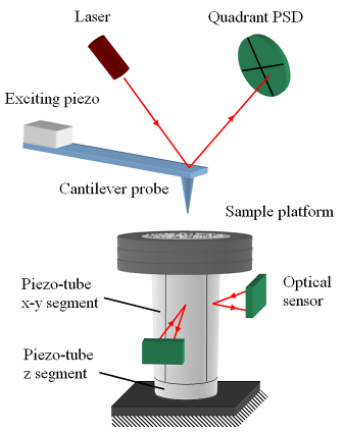

Figure 4.1. *Basic AFM setup: the probe is excited by a piezoelectric element using a sinusoidal wave form. The probe's deflection is measured by sensing the displacement of the laser beam reflected from the tip onto a photo sensor diode. The sample to be scanned is placed on a piezotube. The upper quarter part of the piezotube is used for the raster scan motion in the x–y plane and the lower single part is used for the vertical motion in z*

Having the same reasonable assumption made for the feedforward controllers, this paper focuses on the repetitive control technique which is a powerful way of tracking or rejecting periodic signals [AKS 06]. The organization of the rest of the section is as follows. In section 4.2.1, a tapping mode AFM system scheme is introduced along with a description of the experimental AFM hardware being used. Repetitive control basics and mapping the design specifications into parameter space are explained in sections 4.2.2 and 4.2.3, respectively. The repetitive control features of the COMES are outlined in section 4.2.4. In section 4.2.5, a parameter space-based robust repetitive controller is designed using the COMES toolbox running in Matlab. Simulation results obtained using an accurate and realistic computer model are demonstrated in section 4.2.6.

4.2.1. *Tapping mode AFM system model*

The model used in this part of the chapter on controlling the vertical axis of an AFM stage is based qualitatively on the numerical model in [VAR 08] that was built for simulating a tapping mode AFM. The complete system in [VAR 08] can be redrawn as in Figure 4.2 for control purposes. The scanning probe is vibrated at the frequency of 221 kHz. The excitation signal is adjusted to maintain a free air amplitude of 45 nm and the Q factor is set to 79. The reason for the selection of this Q will be explained later.

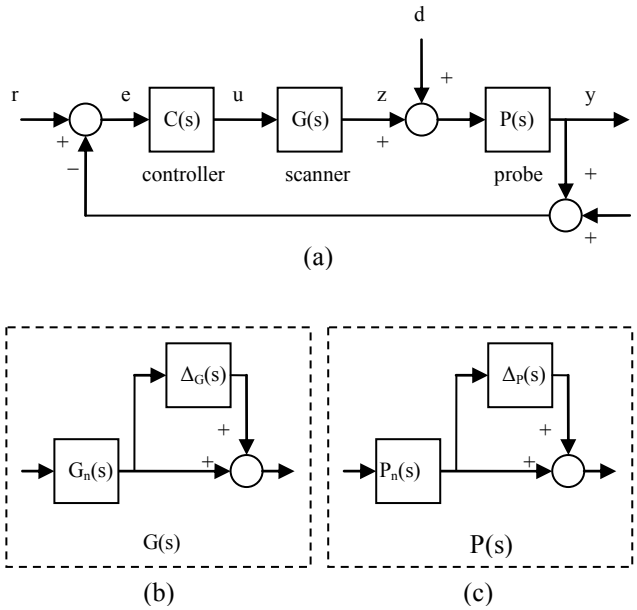

Figure 4.2. *(a) AFM system model in classical control where r is the set amplitude of the probe vibration, y is the actual amplitude, u is the control signal in volts, z is the scanner's vertical motion in nanometers, and d is the surface topography; (b) the uncertainty in the linear scanner model; and (c) the uncertainty in the linear probe model*

The interaction forces between the tip and the sample surface change the amplitude of vibration in tapping mode AFM. Since it is desired to keep these interaction forces unchanged, it is necessary to keep the amplitude of the probe's vibration unchanged. This is achieved by controlling the distance between the tip and the surface by feeding back this amplitude. This is also called constant force scanning. Thus, the probe works like a sensor of interaction forces such that the input is the distance, and the output is the amplitude of the vibration as shown in Figure 4.1.

However, the probe block in Figure 4.2a is not linear. The nonlinearities are due to the attractive and repulsive regimes of the interaction forces, the probe indentation into the sample, and so on [VAR 08]. The reader should note that all of these factors are present in the model that is used for simulations here. It is observed during numerical simulations that the probe shows a quite linear behavior for input signals greater that 10 nm with an approximate DC gain of unity. For those sizes of the inputs, the dynamics can be characterized by a first-order filter due to the sharp 90 degrees phase transition observed at around 3 kHz. The nonlinearities occur such that the DC gain converges to 2 and the dynamics become oscillatory in the order of 2 for closer proximity of the tip to the surface.

We do not want to be concerned with the probe's dynamics at this moment as our aim is to improve the bandwidth of the scanner's vertical axis motion, which typically lies within the 1–40 kHz frequency band. That is why the Q value is chosen to be low. Therefore, we neglect the uncertainties described in Figure 4.2c in the linear analysis and assume a static $P(s) = 1$ model for the probe dynamics since we will discuss the areas satisfying that condition. Note that robust handling of the probe nonlinearities can be achieved using the disturbance observer method presented in section 4.3.

Different from [VAR 08], the stage dynamics is chosen as that of a piezotube actuator here, as given in [OHA 95]. The transfer function of the piezotube's vertical axis motion is given in equation [4.1] where the input is the driving voltage and the output is the displacement along the z-axis in meters.

$$\frac{z_{\text{pt}}(s)}{V_z(s)} = \frac{158.7}{s^2 + 1328s + 1.763 \times 10^{10}} \qquad [4.1]$$

The model in [OHA 95] is derived by curve fitting up to the first mode resonance frequency. The higher frequencies involve uncertainties as is most often the case when a high-order system is modeled using a reduced order representation.

The controller block is designed to keep the output of the feedback loop at the reference value, which is the set amplitude of the probe's vibration. The amplitude is calculated by RMS conversion after 10 oscillations of the probe. The amplitude sensor dynamics are usually of the order of MHz. So, it is safely taken as a static gain in the numerical model.

It is clear from Figure 4.2 that the surface topography is considered as a disturbance that should be rejected. The scanner's motion along the z-axis is recorded while performing the scan operation, thereby obtaining a record of the surface topography also. The complicated AFM system in [VAR 08] is viewed as

a very common and well-known control problem with some assumptions made on the sensor probe and the piezotube actuator. These assumptions lead to simple linear models with uncertainty and the need to use a robust controller.

4.2.2. *Repetitive control basics*

The repetitive control structure is shown in Figure 4.3 where G_n is the nominal model of the plant, Δ_m is the normalized unstructured multiplicative model uncertainty, W_T is the multiplicative uncertainty weighting function, and τ_d is the period of the periodic exogenous signal. *q(s)* and *b(s)* are filters used for tuning the repetitive controller. Repetitive control systems can track periodic signals very accurately and can reject periodic disturbances very satisfactorily. This is due to the fact that the positive feedback loop in Figure 4.4 is a generator of periodic signals with period τ_d for $q(s) = 1$. A low-pass filter with unity DC gain is used for *q(s)* for robustness of stability [HAR 88] and [WEI 97].

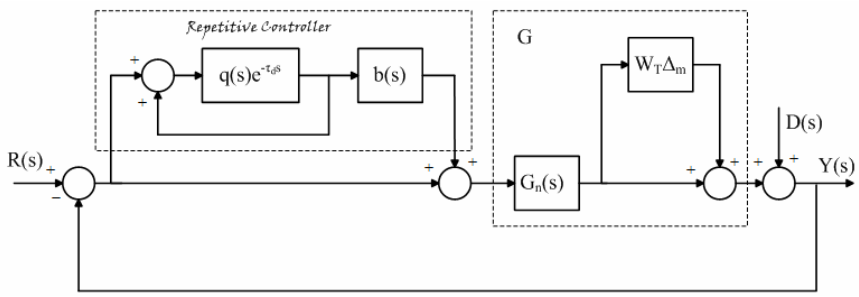

Figure 4.3. *Repetitive contolled system*

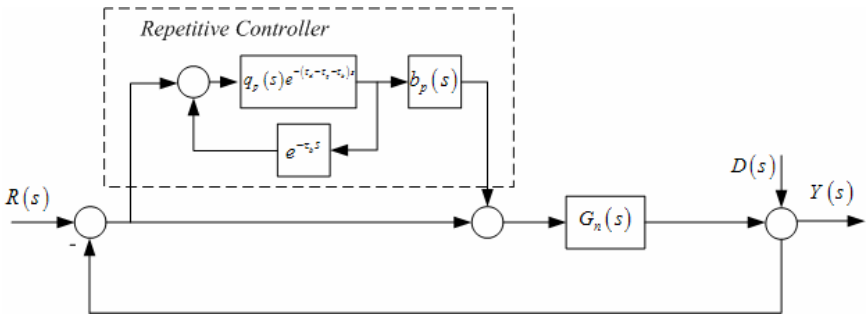

Figure 4.4. *Modified repetitive control system*

The repetitive controller design involves the design of the two filters *q(s)* and *b(s)* in Figure 4.3. In the frequency domain, the ideal low-pass filter *q(jω)* would be unity in the frequency range of interest and zero at higher frequencies. This is not possible and *q(jω)* will have negative phase angle which will make *q(jω)* differ from unity, resulting in reduced accuracy. To improve the accuracy of the repetitive controller, a small time advance is customarily incorporated into *q(s)* to cancel out the negative phase of its low-pass filter part within its bandwidth. This small time advance can easily be absorbed by the much larger time delay τ_d corresponding to the period of the exogenous input signal and does not constitute an implementation problem.

The main objective of the usage of the dynamic compensator *b(s)* is to improve the relative stability, the transient response, and the steady-state accuracy in combination with the unity DC gain low-pass filter *q(s)*. Consider the function of frequency given by:

$$R(\omega) = \left| q(j\omega)\left[1 - b(j\omega)\frac{G(j\omega)}{1+G(j\omega)}\right]\right| \qquad [4.2]$$

which is called the regeneration spectrum in [SRI 91]. According to the same reference, $R(\omega) < 1$ for all ω is a sufficient condition for stability. Moreover, $R(\omega)$ can be utilized to obtain a good approximation of the locus of the dominant characteristic roots of the repetitive control system for large time delay, thus resulting in a measure of relative stability, as well. Accordingly, the compensator $b(s)$ is designed to approximately invert $G/(1+G)$ within the bandwidth of $q(s)$ in an effort to minimize $R(\omega)$. The dynamic compensator $b(s)$ can be selected as only a small time advance or time advance multiplied by a low-pass filter to further minimize $R(\omega)$. To make $R(\omega) < 1$, the time advance in the filter $b(s)$ is chosen to cancel out the negative phase of $G/(1+G)$. This small time advance can easily be absorbed by the much larger time delay τ_d corresponding to the period of the exogenous input signal and does not constitute an implementation problem (Figure 4.4).

The $q(s)$ and $b(s)$ filters are thus expressed as:

$$q(s) = q_p(s)e^{\tau_q s} \qquad [4.3]$$

$$b(s) = b_p(s)e^{\tau_b s} \qquad [4.4]$$

The time advances, τ_q and τ_b, are first chosen to decrease the magnitude of $R(\omega)$ given in equation [4.2]. Then, the design focuses on pairs of chosen parameters in $q_p(s)$ or $b_p(s)$ to satisfy a frequency domain bound on the mixed sensitivity

performance criterion. If L denotes the loop gain of a control system, its sensitivity and complementary sensitivity transfer functions are:

$$S = \frac{1}{1+L} \quad [4.5]$$

$$T = \frac{L}{1+L} \quad [4.6]$$

The parameter space design, presented in the following aims at satisfying the mixed sensitivity performance requirement:

$$\left\| |W_S S| + |W_T T| \right\|_\infty < 1 \text{ or } |W_S S| + |W_T T| < 1 \quad \text{for } \forall \omega \quad [4.7]$$

where W_S and W_T are the sensitivity and complementary sensitivity function weights. The loop gain of the repetitive control system seen in Figures 4.3 and 4.4 are given by:

$$L = G\left(1 + \frac{q_p}{1 - q_p e^{(-\tau_d+\tau_q)s}} b_p e^{(-\tau_d+\tau_q+\tau_b)s}\right) \quad [4.8]$$

The mixed sensitivity design requires:

$$|W_S(\omega)S(j\omega)| + |W_T(\omega)T(j\omega)| = \left|\frac{W_S(\omega)}{1+L(j\omega)}\right| + \left|\frac{W_T(\omega)L(j\omega)}{1+L(j\omega)}\right| < 1 \quad [4.9]$$

or equivalently equation [4.10] to be satisfied for all ω.

$$|W_S(\omega)| + |W_T(\omega)L(j\omega)| < |1 + L(j\omega)| \quad [4.10]$$

4.2.3. *Mapping mixed sensitivity specifications into controller parameter space*

A repetitive controller design procedure based on mapping the mixed sensitivity frequency domain performance specification given in equation [4.10] with an equality sign into the chosen repetitive controller parameter plane at a chosen frequency is described here. Consider the mixed sensitivity problem given in Figure 4.5 illustrating equation [4.10] with an equality sign (called the mixed sensitivity point condition). Apply the cosine rule to the triangle with vertices at the origin, –1 and L in Figure 4.5, to obtain:

$$\left(|W_S(\omega)| + |W_T(\omega)L(j\omega)|\right)^2 = |L(j\omega)|^2 + 1^2 + 2|L(j\omega)|\cos\theta_L \quad [4.11]$$

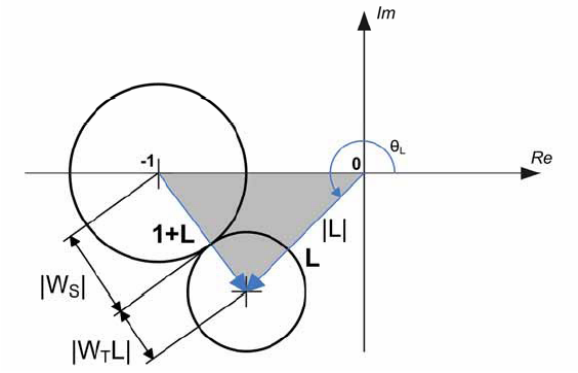

Figure 4.5. *Illustration of the point condition for the mixed sensitivity*

Equation [4.11] is quadratic in $|L(j\omega)|$ and its solutions are:

$$\left|L(j\omega)\right| = \frac{(-\cos\theta_L + \left|W_S(\omega)\right|\left|W_T(\omega)\right|) \pm \sqrt{\Delta_M(\omega)}}{1-\left|W_T(\omega)\right|^2} \qquad [4.12]$$

where:

$$\Delta_M(\omega) = \cos^2\theta_L + \left|W_S(\omega)\right|^2 + \left|W_T(\omega)\right|^2 - 2\left|W_S(\omega)\right|\left|W_T(\omega)\right|\cos\theta_L - 1 \qquad [4.13]$$

Only positive and real solutions for $|L|$ are allowed, that is, $\Delta_M \geq 0$ in equation [4.12] must be satisfied. A detailed explanation of the point condition solution is given in [DEM 10].

4.2.4. *Repetitive control features of COMES*

COMES toolbox is a graphical user interface (GUI) for the routines of four different control approaches [DEM 09]: classical control (lead, lag, PID, and so on), preview control, model regulator control, and repetitive control, which are coded as Matlab M-files. The repetitive control design module of the COMES toolbox is used for determining the parameter space regions corresponding to chosen frequency-domain criteria. The solution technique is based on mapping a frequency domain mixed sensitivity bound into the chosen repetitive controller parameter plane as explained in the previous section. The procedure leads to graphical solution regions in 2D plots for each design specification. A screenshot from the repetitive control design module of COMES is shown in Figure 4.6.

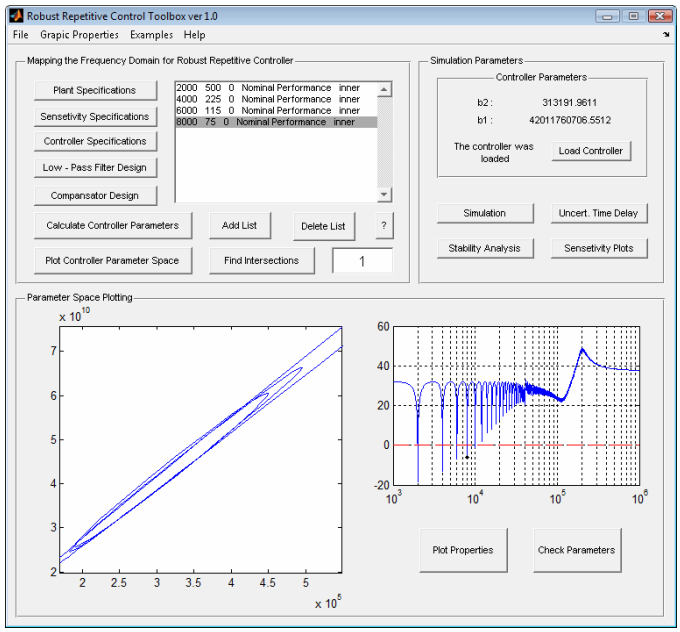

Figure 4.6. *GUI of the repetitive control module of COMES*

First, the plant specifications are introduced. Second, the sensitivity and complementary sensitivity weights are introduced for a range of discrete frequency values. Then, the controller specifications such as the fundamental or the harmonics of the repetitive signal and the number of grid points for the θ sweep in Figure 4.5 are entered. The q filter, which is a second-order low-pass filter with unity DC gain as described previously, is entered parametrically in terms of a_{00} and a_{01}. Then the compensator b is entered as presented previously as well. Finally, the low-pass filter parameters are calculated numerically by the COMES and the solution region satisfying the design criteria is plotted in the parameter space. Having repeated this calculation by updating the sensitivity specifications and the controller specifications for each frequency, new solution regions are plotted on the same plane. The overall solution region satisfying all the design criteria is the intersection of these regions, which is shown with color filling. The q filter parameters are then chosen by the user within the solution region.

The frequency plots of sensitivity, complementary sensitivity, loop gain, and the regeneration spectrum can be observed for convenience using the "Sensitivity Plots" pane. The aim of COMES is to provide a user-friendly toolbox with an interactive GUI that lets all necessary calculations run smoothly in the background while the user can focus on analyzing the graphical results.

4.2.5. *Robust repetitive controller design using the COMES toolbox*

The point condition solution is implemented using the repetitive control module of the COMES toolbox. The design specifications are determined as in Figure 4.7, as good tracking (nominal performance) at low frequencies, mixed sensitivity at intermediate frequencies, and robust stability at high frequencies where unstructured multiplicative uncertainties of the piezotube exist. No performance specification is required near the resonance since the system is not operated at those frequencies.

The weights W_S and W_T are determined for arbitrary frequencies inside the regions in Figure 4.7 as shown in Table 4.1. The design is based on a periodic signal with a fundamental frequency of 200 Hz, hence the repeating period is 0.005 s.

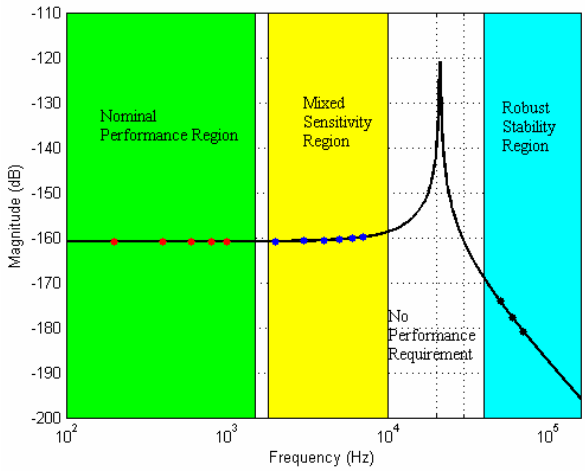

Figure 4.7. *Design specifications for the repetitive controller*

Having determined the design specifications in Table 4.1, the filter $b(s)$ is designed as in [4.14], and $q(s)$ is chosen to be in the form of [4.15]. The parameters a_{00} and a_{01} in [4.15] must be appropriately selected from the parameter space to satisfy the design specifications given in Figure 4.7 and Table 4.1. The solution regions of the point condition on the parameter space are plotted in Figure 4.8 for each frequency given in Table 4.1. The intersection of those regions is color filled and an arbitrary point somewhere near the center of this intersection is selected to determine a_{00} and a_{01} that are given in [4.16].

$$b(s) = \frac{6.707\times10^{7}s^{2} + 1.591\times10^{14}s + 1.104\times10^{18}}{s^{2} + 2\times10^{5}s + 10^{10}} \qquad [4.14]$$

$$q(s) = \frac{a_{00}}{s^2 + a_{01}s + a_{00}} \quad [4.15]$$

$$a_{00} = 3.8882 \times 10^8; \quad a_{01} = 2.9133 \times 10^4 \quad [4.16]$$

Finally, time advances τ_b=6.268×10^{-6}s and τ_q=7.5×10^{-5}s are calculated to compensate for the phase lags introduced by $q(s)$ and $b(s)G(s)/[1+G(s)]$ as shown in Figure 4.9.

$f = k/\tau_d$ (Hz)	k	W_S	W_T
200	1	500	0
400	2	250	0
600	3	115	0
800	4	60	0
1,000	5	40	0
3,000	15	3	0.02
4,000	20	1.9	0.02
5,000	25	1.45	0.02
6,000	30	1.25	0.05
7,000	35	1.1	0.05
50,000	250	0	0.2
60,000	300	0	0.2
70,000	350	0	0.2

Table 4.1. *Weights for controller design (τ_d = 0.005 which is the period of the repetitive signal)*

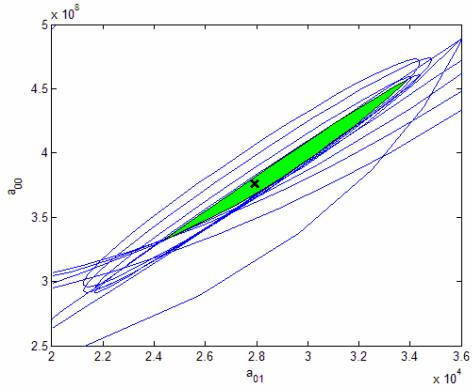

Figure 4.8. *Solution regions of the point condition*

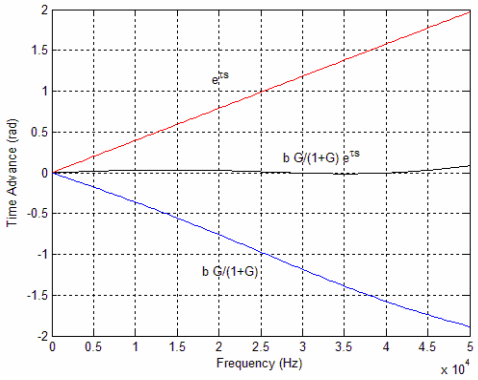

Figure 4.9. *Compensation of the phase lag by time advance*

4.2.6. *Simulation results for the vertical direction*

Numerical simulations are used to evaluate the repetitive controller designed for the vertical axis of the piezotube-based AFM. A square wave input of 40 nm height at 200 Hz is assumed to be the surface topography being scanned. The result obtained using a well-tuned PI controller for the vertical motion of the piezotube is illustrated in Figure 4.10a and the error is shown in Figure 4.10b. The oscillations occur due to the insufficient bandwidth of the system as was mentioned earlier.

Figure 4.11a illustrates the scan simulation under repetitive control instead of the PI controller and the corresponding error is shown in Figure 4.11b. Apparently, the scan obtained with the repetitive controller is better than the PI after the first two periods. The error is smaller at the moments of disturbances (step changes in surface topography) and so is the control effort as a consequence.

Another important factor in constant force scanning is the size of the interaction forces between the probe's tip and the sample surface. Large forces are not convenient to avoid probable damage on the tip and the sample, especially when the sample is made of organic matter like a biological specimen. The comparison of the interaction forces with the PI and the repetitive controller are demonstrated in Figure 4.12. After the first period, the forces are reduced considerably both on the flat parts of the steps and at the moments of disturbances when more control effort is needed.

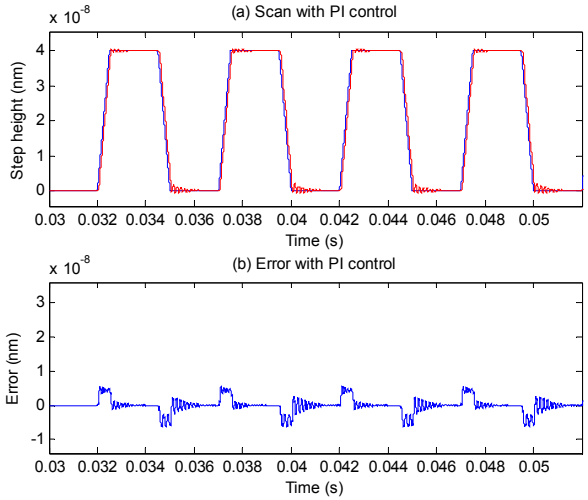

Figure 4.10. *Illustration of the scan with PI control (a) and the error on the probe's oscillation amplitude (b)*

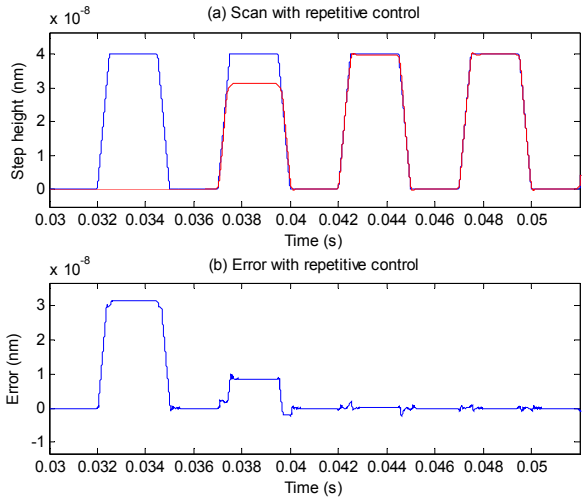

Figure 4.11. *Illustration of the scan with repetitive control (a) and the error on the probe's oscillation amplitude (b)*

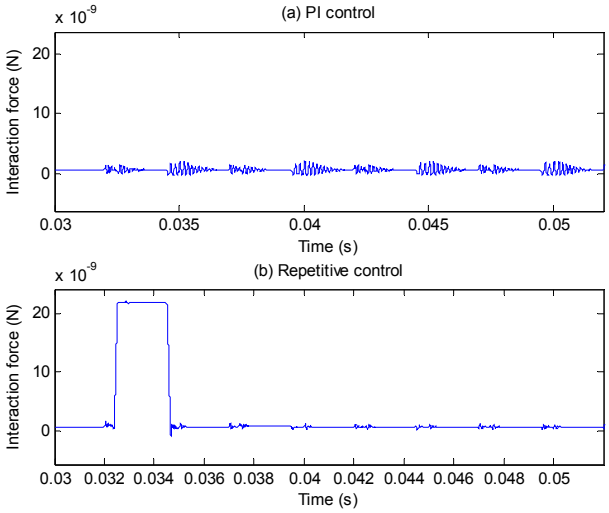

Figure 4.12. *Illustration of the interaction forces in the case of PI control (a) and the same forces in the case of repetitive control (b)*

4.3. MIMO disturbance observer control of the lateral directions

To illustrate different possible robust control methods that can be applied to AFM axes of motion, a disturbance observer is applied to the lateral scanning axes of a piezotube-based AFM in this section. Piezoelectric materials are widely used to obtain accurate motion of its axes, offering sub-nanometer precision. Tube-shaped piezoelements are commonly used as actuators because they are very good manipulators with their compact design, three degrees of freedom, low cost, and good properties for control purposes like stability, fast response, high bandwidth, and high precision. However, they also present undesired behavior like hysteresis, creep, thermal drift, and coupled motion of their axes [MOH 08], [DEV 07]. In particular, this coupled motion of the axes requires special attention when a piezoelectric tube actuator is used as a scanner for an AFM as it results in inaccuracies in absolute positioning and causes image distortions.

It is observed for most of the piezotubes that there is a coupling between the *x*- and *y*-axes, due to the inevitable eccentricity of the inner and outer cylinders of the tube as shown in Figure 4.13, which occurs during manufacturing. Moreover, there is a cross-coupling between the lateral and the vertical axes (not discussed here) which causes imaging inaccuracy when large areas are scanned. A piezostack actuated stage can be used as the nanopositioner instead of a piezotube to reduce the coupling effects [SAL 02]. However, it needs more complicated and expensive mechanical design to obtain three degrees-of-freedom motion. This complicated

mechanical design may result in highly coupled motion of the axes while offering higher bandwidth [DON 07].

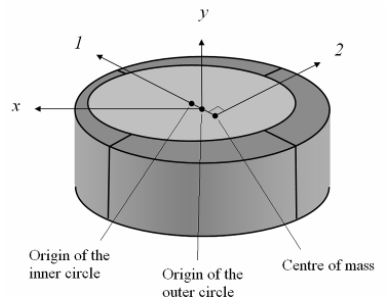

Figure 4.13. *x and y are the theoretical axes of motion whereas 1 and 2 are the actual axes of motion, the difference being caused by the eccentricity of the inner and the outer walls of the tube*

Previous work has been carried out in [TIE 04], [TIE 05] to compensate for the errors caused by the cross-coupling using inversion-based iterative control approach. However, the undesired motion in the lateral axes caused by the coupling between the *x*- and *y*-directions remains, as it causes image distortions in the *x*–*y* plane and prevents absolute positioning for all sizes of the scan area.

[DAN 99] published their work that handles the lateral coupling problem by a MIMO controller with lateral feedback where a particular controller is designed for the ramp-type input signals used for triangular scan motion only. A more recent work is presented by Yong *et al.* [YON 10] on the lateral coupling problem of a piezostack actuated stage by using H_∞ controller design.

In fact, the coupling between the lateral axes has been customarily compensated for by introducing a variety of correction polynomials after an open-loop calibration process for commercial AFMs, rather than by using the above-mentioned control solutions. In this section, we propose a different method by offering an add-on digital control unit with an embedded algorithm that uses the *MIMO disturbance observer control* method of [AKS 10], for canceling the coupling between the lateral axes *x* and *y* of a piezotube by designing appropriate filters. One of the main contributions of the use of this control strategy is that the primary scans and iterations, which are not practical when manipulation of a particle instead of imaging of a surface is the case, are not necessary for learning purposes before imaging. Besides, this control strategy is not restricted to a certain type of input signal and hence can be used for motion profiles that have non-repetitive and/or unbiased trajectories. Moreover, the decoupling controller system proposed here is easy to tune.

An accurate model of the piezoelectric tube actuator is needed as a pre-requisite for control analysis and design. Previous work on linear models for ideal uncoupled lateral motion of the piezotube actuator has been published in [RAT 05] and an analytical model has been derived in [OHA 95]. A coupled analytical model has also been published in [RIF 01]. A fast, robust nanopositioning application has been treated in [LEE 09] using a two controller degrees-of-freedom LMI-based controller.

In this section, a MIMO model is used for the controller design. This MIMO model has been derived experimentally and contains the coupling effects between the lateral axes, as well. The organization of the rest of the section is as follows: in section 4.3.1, the experimental setup and the model of the quartered piezotube for lateral dynamics are given, whereas section 4.3.2 presents the basics and analysis of the MIMO disturbance observer algorithm used. In section 4.3.3, the design of a suitable controller and experimental results are given for the controlled and uncontrolled motions of the piezotube. The chapter ends with concluding remarks in section 4.4.

4.3.1. *The piezotube and the experimental setup*

The structure in Figure 4.14 is a custom built system where infrared sensors (Sharp GP2S60) are placed on the *x*- and *y*-axes for feedback. The infrared light is reflected from the body of the tube (Figure 4.1) onto a phototransistor output, which is a reflective photointerrupter with emitter and detector facing the same direction in a molding that provides non-contact sensing. It also blocks visible light to minimize false detection. The piezotube is placed on a granite plate to protect it against environmental vibrations. It is manipulated by a digital controller using the analog to digital converter (ADC), digital to analog converter (DAC), and a processor mounted on the digital control unit. A schematic representation of the system is sketched in Figure 4.15a and the corresponding picture of the setup is shown in Figure 4.15b. The calibration free decoupling algorithm (the MIMO disturbance observer) runs on the add-on digital control unit as shown in Figure 4.15a. The piezotube is placed in an acoustic enclosure to protect the whole AFM process against environmental sounds.

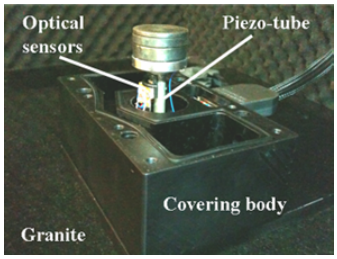

Figure 4.14. *Piezotube placed on granite with optical sensors measuring x- and y-axes motion*

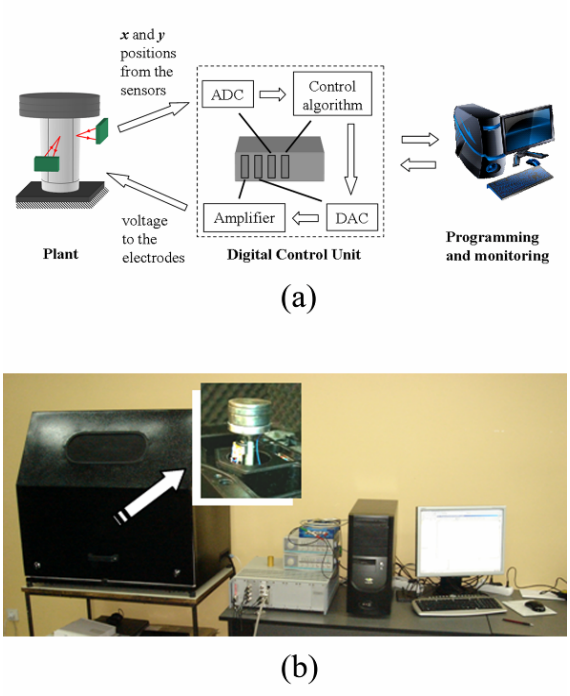

Figure 4.15. *(a) Schematic diagram and (b) the picture of the experimental setup and the hardware*

The dynamical behavior of the piezotube can be characterized as a well-known mass-spring-damper system, thanks to its structure. The sampling rate is 1 kHz because of the hardware conditions and discrete methods are used for system identification, analysis, and control. The whole system is modeled as given in equations [4.17]–[4.22]. The input is the digital value corresponding to the voltage output of the 18-bit DAC such that a unit increment equals 7.63×10^{-5} volts. Similarly, the output is the digital value corresponding to the voltage input of the 16-bit ADC such that a unit increment equal to 2.9×10^{-4} volts corresponds to a 10 nm displacement. The amplifier gain for the high voltage applied to the electrodes is 10.

The transfer functions in [4.19]–[4.22] are calculated by least squares curve fitting over the time responses of the system to various test signals, as they represent the direct throughputs and the undesired coupling effects, respectively. Note that the denominators of the direct throughputs [4.19] and [4.20] are essentially the same as expected because they arise from the same mechanical system. The denominators in the coupling effect transfer functions [4.21] and [4.22] are slightly different which is

due to the fact that the coupled motion is small. Therefore, their estimation is not as accurate as in [4.19] and [4.20]. This situation does not constitute any problem since the coupling dynamics are only a measure of the model uncertainties to be robustly handled by the controller, and the direct throughput functions are essentially used for the controller design.

$$\begin{bmatrix} x \\ y \end{bmatrix} = \underbrace{\begin{bmatrix} G_{xx}(z) & G_{yx}(z) \\ G_{xy}(z) & G_{yy}(z) \end{bmatrix}}_{G(z)} \cdot \begin{bmatrix} u_x \\ u_y \end{bmatrix} \qquad [4.17]$$

$$G_{ij}(z) = \frac{j(z)}{u_i(z)} = \frac{b_{0ij}}{z^2 + a_{1ij}z + a_{0ij}} \quad \text{for } i = x,\ y \text{ and } j = x,\ y \qquad [4.18]$$

$$G_{xx}(z) = \frac{x(z)}{u_x(z)} = \frac{-0.0057}{z^2 - 1.5017z + 0.9331} \qquad [4.19]$$

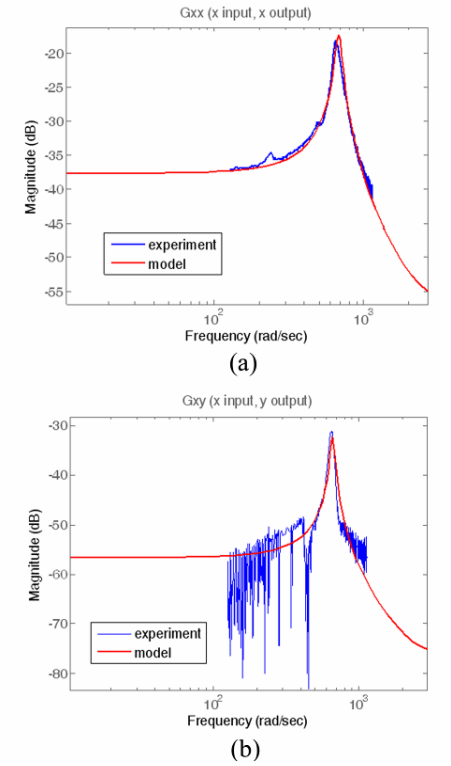

Figure 4.16. *(a) Frequency response from x to x, (b) frequency response from x to y. Similar plots are obtained from y to y and y to x as a function of applied field*

$$G_{yy}(z) = \frac{y(z)}{u_y(z)} = \frac{0.0044}{z^2 - 1.4995z + 0.9286} \quad [4.20]$$

$$G_{xy}(z) = \frac{y(z)}{u_x(z)} = \frac{0.0006}{z^2 - 1.5480z + 0.9596} \quad [4.21]$$

$$G_{yx}(z) = \frac{x(z)}{u_y(z)} = \frac{0.0005}{z^2 - 1.5160z + 0.9922} \quad [4.22]$$

Superimposed plots of the frequency responses of the piezotube and the model functions, which are obtained from the frequency sweep up to 200 Hz and impulse responses, respectively, are given in Figure 4.16.

4.3.2. *MIMO disturbance observer*

The MIMO disturbance observer algorithm used for calibration free decoupled motion is presented in this section. The disturbance observer is a two degrees-of-freedom control system inside the control unit that makes an uncertain plant behave like its nominal or desired model. It also has excellent disturbance rejection properties. The coupling caused dynamics on a certain axis of the piezotube is treated as model uncertainty here and the MIMO disturbance observer is used to decouple the lateral axes of scanning. Consider plant P with multiplicative model error $W_m\Delta_m$ and external disturbance d. Note that the "y" term in the equations from [4.23] to [4.34] in the following discussion is the general output of the control system, not the y-axis. The input–output relation is expressed as follows:

$$y = Pu + d = (P_n(I + W_m\Delta_m))u + d \quad [4.23]$$

where P_n is the nominal (or desired) model of the plant. P and P_n are square transfer function matrices of dimension two here and I is the identity matrix of dimension two. P_n is chosen as a non-singular and diagonal matrix as follows:

$$P_n = \begin{bmatrix} P_{n1} & 0 \\ 0 & P_{n2} \end{bmatrix} \quad [4.24]$$

The aim of the disturbance observer is to obtain:

$$y = P_n u_n \quad [4.25]$$

as the input–output relation which is called model regulation. Model regulation will allow the individual piezoelectric tube scanning axes to be decoupled as the desired

model P_n in [4.25], with P_{n1} and P_{n2} in [4.24] being the decoupled *x*- and *y*-axes transfer functions, respectively. Doing this, we can achieve the desired response from the plant, that is, the *x*- and *y*-axes of the piezoelectric tube. The diagonal form of the transfer function matrix in the nominal model is critical for decoupling purposes since the original MIMO problem is divided into two independent SISO problems with this choice.

The extended error is defined by putting the external disturbance and the model uncertainty together and reformulating [4.23] as follows:

$$y = (P_n(I + W_m\Delta_m))u + d = P_n u + e,\ e = P_n W_m \Delta_m u + d \quad [4.26]$$

which can be re-expressed as:

$$e = y - P_n u \quad [4.27]$$

The effect of the extended error in [4.26] can be canceled using the following control law:

$$u = u_n - P_n^{-1} e = u_n - P_n^{-1} y + u \quad [4.28]$$

which achieves the model regulation aim in [4.25].

However, P_{n1}^{-1} and P_{n2}^{-1} required when calculating the inverse of P_n in [4.28] are not causal and hence cannot be implemented. Therefore, we pre-multiply it by a low-pass filter *Q* in the following form:

$$Q = \begin{bmatrix} Q_1 & 0 \\ 0 & Q_2 \end{bmatrix} \quad [4.29]$$

to make the diagonal elements of the 2 × 2 matrix QP_n^{-1}, namely Q_1/P_{n1} and Q_2/P_{n2} causal.

Including the sensor noise as well, $y + n$ is used instead of *y* for the actual output signal and the new control law becomes:

$$u = u_n - QP_n^{-1}(y + n) + Qu \quad [4.30]$$

The block diagram of the above-mentioned control scheme is shown in Figure 4.17.

With this approach, two independent SISO loops can be designed with the nominal models P_{ni} and the Q_i filters with the above choice of [4.24] and [4.29] where i=1, 2. Usually, u_n is chosen to be a triangular wave on one axis while it is a ramp on the other axis to provide the raster scan motion.

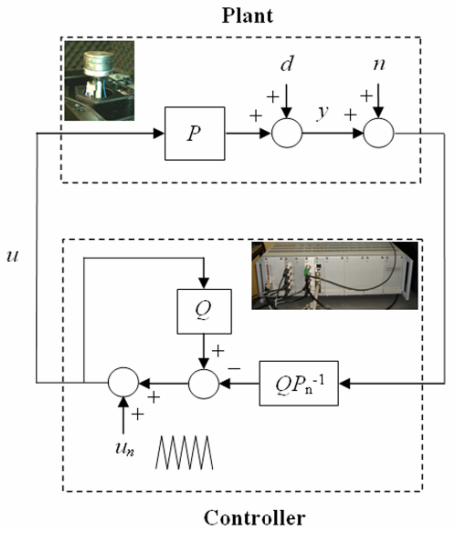

Figure 4.17. *MIMO disturbance observer architecture*

4.3.3. *Disturbance observer design for the piezotube and experimental results*

Note the following relation of the control scheme in Figure 4.17 between its inputs and output.

$$y = [I + P(I-Q)^{-1}QP_{\mathrm{n}}^{-1}]^{-1}[P(I-Q)^{-1}u_{\mathrm{n}} + d - P(I-Q)^{-1}QP_{\mathrm{n}}^{-1}n] \qquad [4.31]$$

Using [4.31] and some manipulations, the input–output relation from u_{n} to y is as follows:

$$\frac{y}{u_{\mathrm{n}}} = [(I-Q)P^{-1} + QP_{\mathrm{n}}^{-1}]^{-1} \qquad [4.32]$$

The expression in [4.32] is equal to P when Q=0 and is equal to P_{n} when Q=I, which shows that model regulation is perfect for Q=I, the 2×2 identity matrix. Similarly, the input–output relation from d to y is:

$$\frac{y}{d} = I - P[(I-Q) + QP_{\mathrm{n}}^{-1}P]^{-1}QP_{\mathrm{n}}^{-1} \qquad [4.33]$$

and that is equal to the zero matrix when Q=I, which means perfect disturbance rejection. In addition to that, the input–output relation from n to y is:

$$\frac{y}{n} = -[I + P(I-Q)^{-1}QP_{\mathrm{n}}^{-1}]^{-1}[P(I-Q)^{-1}QP_{\mathrm{n}}^{-1}] \qquad [4.34]$$

Equation [4.34] is equal to the zero matrix when Q=0, which means perfect sensor noise rejection.

Since our aim is to decouple the motion along the lateral axes, the nominal models can be chosen such that $P_{n1} = G_{xx}$ and $P_{n2} = G_{yy}$ as given in [4.35].

$$P_{n1} = \frac{-0.0057}{z^2 - 1.502z + 0.9331}$$
$$P_{n2} = \frac{0.0044}{z^2 - 1.499z + 0.9286} \qquad [4.35]$$

Considering the results above, Q_i, for i=1, 2 are chosen to be low-pass filters with unity DC gain which provide model regulation and disturbance rejection at low frequencies and sensor noise rejection at high frequencies. Basically, $Q_1 = Q_2$ and the poles are placed at 100 Hz and 120 Hz as in [4.36]. Thus, the frequencies within the operating frequency range of the piezotube, which is below its resonant frequency, are covered and the rest are filtered out. Figure 4.18 demonstrates the frequency response plots of P_{n1}, P_{n2}, and $Q_{1,2}$.

$$Q_i = \frac{0.247}{z^2 - 1.004z + 0.251} \qquad [4.36]$$

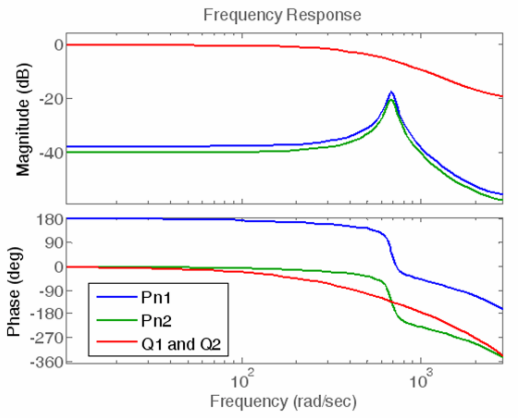

Figure 4.18. *Frequency response plots of the P_{n1}, P_{n2}, and $Q_{1,2}$ designed for the piezotube*

The corresponding difference equations are embedded into the digital control unit to implement the loop in Figure 4.17 using the designed filters. The following tests are carried out to see the results of the controlled and the uncontrolled cases.

Figure 4.19 demonstrates the decoupling ability of the MIMO disturbance observer controller for a step input in the *x*-direction. Although this input results in undesired coupled motion in the *y*-direction in the uncontrolled case, this undesired effect vanishes in the controlled case as illustrated in the experimental response of Figure 4.19. Figures 4.20 and 4.21 show the motion of the piezotube when rectangular and circular trajectories, respectively, in the *x*–*y* plane are desired. It is seen from Figure 4.20 that the rectangular trajectories are not coincident in the uncontrolled case. This is due to the hysteresis effect that is revealed significantly on the *y*-axis, which causes each rectangle to appear shifted on *y* (i.e. 2 in the coupled case, Figure 4.13). Besides, the *x*- and *y*-axes motions are rotated due to the eccentricity of the piezotube. Note that the simulation model represents the rotation of the axes (i.e. the coupling), but not the shifting of the rectangles because the hysteresis effect is not governed by this model. However, in the controlled case, the rectangles are not rotated thanks to the decoupled motion of the lateral axes and they are all coincident as desired. This shows that the undesired hysteresis effect is also handled by the MIMO disturbance observer successfully, as well as the coupling problem.

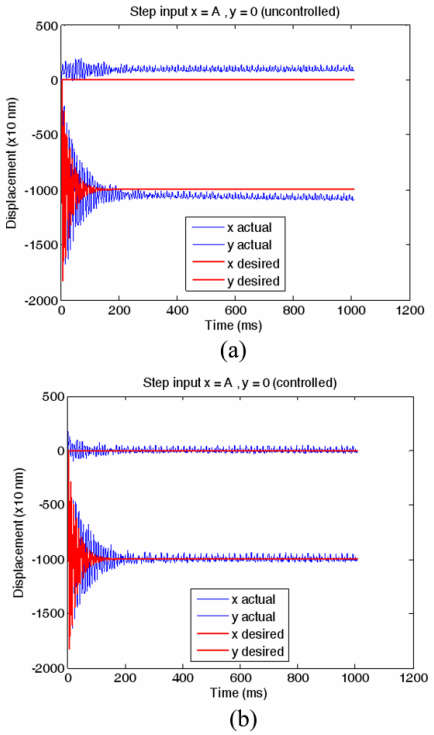

Figure 4.19. *Responses of the x- and y-axis in (a) the uncontrolled and (b) the controlled cases for a step input only on x*

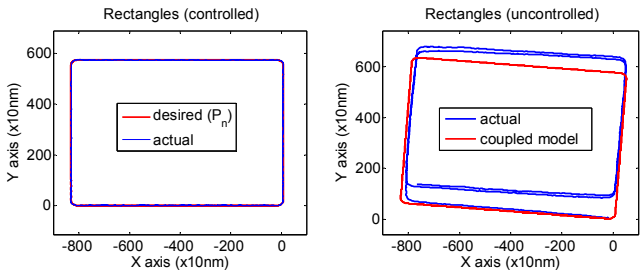

Figure 4.20. *Rectangular motion of the piezotube on x–y plane in (a) the uncontrolled and (b) the controlled cases*

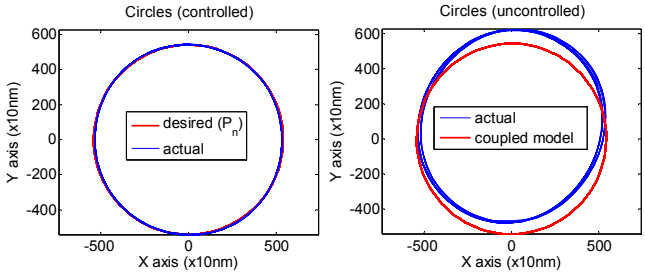

Figure 4.21. *Circular motion of the piezotube on x–y plane in (a) the uncontrolled and (b) the controlled cases*

The performance of the method is tested by a circular motion in the *x–y* plane, and the results are shown in Figure 4.19. In the uncontrolled case, it is seen that the center is not at the origin (zero) because of the hysteresis effect and the circles are shifted on *y* (i.e. 2 in the coupled case, Figure 4.13). However, the circles are just as desired in the controlled case. Here, the speed of the circular motion is 10 Hz.

An illustration of a sample scan is presented in Figure 4.22 to emphasize the difference between the coupled and the uncoupled imaging. The sample is artificially created on the computer as having square steps on its surface. The artificial sample surface consists of 550 × 550 points. A usual scan motion is experimented on the piezotube such that it is moved back and forth on *x*, while small steps advances are used on *y*.

The surface height (*z* position) corresponding to each *x* and *y* position of the piezotube are recorded for the illustration of the controlled and the uncontrolled cases. The results are plotted in 3D. It is seen from the figure that the image is

distorted because of the coupling in the uncontrolled case. In addition, the heights of the square steps seem to be larger than they really are. Because the piezotube scans a smaller area than it should due to the hysteresis on *y*, the appearance of that area is stretched out during the imaging process (Figure 4.22).

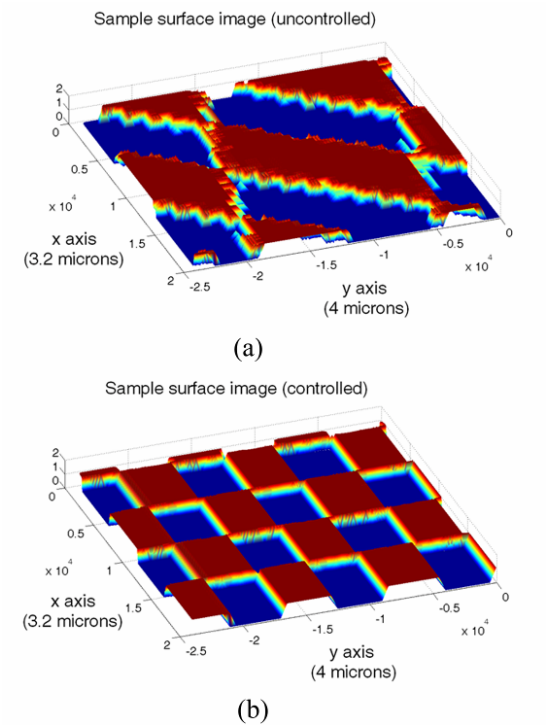

Figure 4.22. *Illustration of an artificial sample surface imaging in (a) the uncontrolled and (b) the controlled cases*

4.4. Concluding remarks

Robust control methods for the vertical and the lateral axes of a piezotube actuator used in an AFM were presented in this chapter. Control of the piezotube in the vertical axis and the lateral axes was treated separately to present two different approaches. Repetitive control was presented in combination with the vertical direction and MIMO disturbance observer control was presented in combination with the lateral axes. Simulations based on a realistic model were used to illustrate the results for the vertical axis and experiments were used for illustrating the results for the lateral axes. The COMES toolbox was used in both cases to fine tune the controller parameters (not shown here in the disturbance observer case for the sake

of brevity) to satisfy mixed sensitivity-type performance specifications. The results presented demonstrate the applicability of these control techniques to AFM control. Note that the disturbance observer can be applied to the vertical axis also. Similarly, repetitive control can be applied to the lateral axes, preferably after MIMO disturbance observer compensation for better performance.

It is seen from the experimental results for the lateral axes that the MIMO disturbance observer works well for calibration free decoupling purposes. Hence, neither correcting factors nor pre-defined polynomials are required to avoid the distorted images. In addition, calibration of the absolute displacement of the axes is no longer necessary since they are forced to obey a nominal model and the desired response is pre-defined in that model. Therefore, the authors conclude that absolute positioning can be offered by having feedback on the orthogonal axes using appropriate sensors and controller hardware installed in the electronics of the conventional AFM.

Besides AFM imaging, the cancelation of the coupling of the axes is very important for manipulation of objects using a piezotube. In this case, the piezotube can be considered as a flexible robot arm where the motion along its axes is controlled satisfactorily by utilization of the MIMO disturbance observer algorithm in the digital control unit.

4.5. Acknowledgments

Section 4.1 that discusses the use of repetitive control in AFM including Figures 4.1–4.12 and Table 4.1 is taken from the ASME paper “Fast AFM Scanning with Parameter Space Based Robust Repetitive Control Designed Using The Comes Toolbox”, by Serkan Necipoglu, Burak Demirel, Levent Güvenç, ESDA 2010 Engineering Systems Design and Analysis Conference, Paper Number ESDA2010-24499. The authors thank ASME for giving them permission to use that paper in this chapter.

The authors would like to thank TÜBİTAK, the Scientific and Technological Research Council of Turkey, for partial support for the second part of the work presented here through grant 108E256. The authors would like to thank Dr Ahmet Oral and Nanomagnetics Inc. for preparing the custom-made AFM piezotube used in the experiments here.

The authors would like to thank Prof. Cagatay Basdogan and the members of his research group at Koc University for cooperation and fruitful discussions on AFM and AFM control.

4.6. Bibliography

[ABR 07] ABRAMOVITCH D.Y., ANDERSSON S.B., PAO L.Y., SCHITTER G., "A tutorial on the mechanisms, dynamics, and control of atomic force microscopes", *Proceedings of American Control Conference*, New York, 2007.

[AKS 06] AKSUN GÜVENÇ B., GÜVENÇ L., "Robust repetitive controller design in parameter space", *ASME Journal of Dynamic Systems, Measurement and Control*, vol. 128, no. 2, 2006, pp. 406–413.

[AKS 10] AKSUN GÜVENÇ B., GÜVENÇ L., KARAMAN S., "Robust MIMO disturbance observer analysis and design with application to active car steering", *International Journal of Robust and Nonlinear Control*, Wiley, vol. 20, 2010, pp. 873–891.

[BIN 86] BINNIG G.K., QUATE C.F., GERBER C., "Atomic force microscope", *Physical Review Letters*, vol. 56, 1986, pp. 930–933.

[DAN 99] DANIELE A., SALAPAKA S., SALAPAKA M.V., DAHLEH M., "Piezoelectric scanners for atomic force microscopes: Design of lateral sensors, identification and control", *Proceedings of American Control Conference*, San Diego, CA, USA, 1999, pp. 253–257.

[DEM 09] DEMIREL B., Development of an interactive design tool for parameter space based robust repetitive control, M.S. Thesis, Istanbul Technical University, Istanbul, Turkey.

[DEM 10] DEMIREL B., GÜVENÇ L., "Parameter space design of repetitive controllers for satisfying a mixed sensitivity performance requirement", *IEEE Transactions on Automatic Control*, vol. 55, no. 8, 2010, pp. 1893–1899.

[DEV 07] DEVASIA S., ELEFTHERIOU E., MOHEIMANI S.O.R., "A survey of control issues in nanopositioning", *IEEE Transactions on Control Systems Technology*, vol. 15, no. 5, 2007, pp. 802–823.

[DON 07] DONG J., SALAPAKA S.M., FERREIRA P.M., "Robust MIMO control of a parallel kinematics nano-positioner for high resolution high bandwidth tracking and repetitive tasks", *Proceedings of 46th IEEE Conference on Decision and Control*, New Orelans, Louisiana, 2007, pp. 4495–4500.

[FUJ 08] FUJIMOTO H., OSHIMA T., "Nanoscale servo control of contact-mode AFM with surface topography learning observer", *10th IEEE International Workshop on Advanced Motion Control*, 2008, pp. 568–573.

[GAR 02] GARCIA R., PEREZ R., "Dynamic atomic force microscopy methods", *Surface Science Reports*, Elsevier Science B.V., vol. 47, 2002, pp. 197–301.

[GUN 07] GUNEV I., VAROL A., KARAMAN S., BASDOGAN C., "Adaptive Q control for tapping mode nanoscanning using a piezoactuated bimorph probe", *Review of Scientific Instruments*, vol. 78, 043778, American Institute of Physics, 2007.

[HAR 88] HARA S., YAMAMOTO Y., OMATA T., NAKANO M., "Repetitive control systems: a new type servo system for periodic exogenous signals", *IEEE Transactions on Automatic Control*, vol. 33, 1988, pp. 657–667.

[LEE 09] LEE C., SALAPAKA S.M., "Fast robust nanopositioning-a linear-matrix-inequalities-based optimal control approach", *IEEE/ASME Transactions on Mechatronics*, vol. 14, no. 4, 2009, pp. 414–422.

[LI 08] LI Y., BECHHOEFER J., "Feedforward control of a piezoelectric flexure stage for AFM", *Proceedings of American Control Conference*, Seattle, Washington, 2008.

[MOH 08] MOHEIMANI S.O.R., "Invited review article: accurate and fast nanopositioning with piezoelectric tube scanners: emerging trends and future challenges", *Review of Scientific Instruments*, vol. 79, 071101, 2008.

[OHA 95] OHARA T., YOUCEF-TOUMI K., "Dynamics and control of piezotube actuators for subnanometer precision applications", *Proceedings of the American Control Conference*, Seattle, Washington, 1995, pp. 3808–3812.

[ORU 09] ORUN B., NECIPOGLU S., BASDOGAN C., GÜVENÇ L., "State feedback control for adjusting the dynamic behavior of a piezo-actuated bimorph AFM probe", *Review of Scientific Instruments*, vol. 80, no. 1, American Institute of Physics, 2009, pp. 063701-1–063701-7.

[PAO 07] PAO L.Y., BUTTERWORTH J.A., ABRAMOVITCH D.Y., "Combined feedforward/feedback control of atomic force microscopes", *Proceedings of the American Control Conference*, New York, 2007.

[RAT 05] RATNAM M., BHIKKAJI B., FLEMING A.J., MOHEIMANI S.O.R., "PPF control of a piezoelectric tube scanner", *Proceedings of the 44th IEEE Conference on Decision and Control, and the European Control Conference*, Seville, Spain, 2005, pp. 1168–1173.

[RIF 01] EL RIFAI O.M., YOUCEF-TOUMI K., "Coupling in piezoelectric tube scanners used in scanning probe microscopes", *Proceedings of the American Control Conference*, Arlington, Virginia, 2001, pp. 3251–3255.

[SAL 02] SALAPAKA S., SEBASTIAN A., CLEVELAND J.P., SALAPAKA M.V., "High bandwidth nano-positioner: A robust control approach", *Review of Scientific Instruments*, vol. 73, no. 9, 2002, pp. 3232–3241.

[SAL 05] SALAPAKA S.M., DE T., SEBASTIAN A., "A robust control based solution to the sample-profile estimation problem in fast atomic force microscopy", *International Journal of Robust and Nonlinear Control*, vol. 15, 2005, pp. 821–837.

[SCH 01] SCHITTER G., MENOLD P., KNAPP H.F., ALLGÖWER F., STEMMER A., "High performance feedback for fast scanning atomic force microscopes", *Review of Scientific Instruments*, vol. 72, no. 8, American Institute of Physics, 2001.

[SCH 04] SCHITTER G., ALLGÖWER F., STEMMER A., "A new control strategy for high-speed atomic force microscopy", *Nanotechnology*, Institute of Physics Publishing, vol. 15, 2004, pp. 108–114.

[SCH 07] SCHITTER G., ASTRÖM K.J., DEMARTINI B.E., THURNER P.J., TURNER K.L., HANSMA P.K., "Design and modeling of a high-speed AFM scanner", *IEEE Transactions on Control Systems Technology*, vol. 15, no. 5, 2007.

[SRI 97] SRINIVASAN K., SHAW F.R., "Analysis and design of repetitive control systems using the regeneration spectrum", *ASME Journal of Dynamical Systems*, *Measurement and Control*, vol. 113, 1991, pp. 216–222.

[SUL 02] SULCHEK T., YARALIOGLU G., QUATE C.F., "Characterization and optimization of scan speed for tapping-mode atomic force microscopy", *Review of Scientific Instruments*, vol. 73, no. 8, American Institute of Physics, 2002.

[TIE 04] TIEN S., ZOU Q., DEVASIA S., "Control of dynamics-coupling effects in piezo-actuator for high-speed AFM operation", *Proceedings of 2004 American Control Conference*, Boston, MA, USA, 2004, pp. 3116–3121.

[TIE 05] TIEN S., ZOU Q., DEVASIA S., "Iterative control of dynamics-coupling-caused errors in piezoscanners during high-speed AFM operation", *IEEE Transanctions Control Systems Technology*, vol. 13, no. 6, 2005, pp. 921–931.

[VAR 08] VAROL A., GUNEV I., ORUN B., BASDOGAN C., "Numerical simulation of nano scanning in intermittent-contact mode AFM under Q control", *Nanotechnology*, vol. 19, 2008, pp. 075503-1–075503-10.

[WEI 97] WEISS G., "Repetitive control systems: old and new ideas", in BYRNES, C., DATTA, B., GILLIAM, D., MARTIN C. (eds), *Systems and Control in the 21st Century*, PSCT, Birkhäuser, Boston, 22, 1997, pp. 389–404.

[YON 10] YONG Y.K., LIU K., MOHEIMANI S.O.R., "Reducing cross-coupling in a compliant xy nanopositioner for fast and accurate raster scanning", *IEEE Transactions on Control Systems Technology*, vol. 18, no. 5, 2010, pp. 1172–1179.